UNIVERSITY OF LEEDS

This is a repository copy of *Detonation shock dynamics of type Ia supernovae*.

White Rose Research Online URL for this paper:
http://eprints.whiterose.ac.uk/82600/

Version: Published Version

Article:

White Rose
university consortium
Universities of Leeds, Sheffield & York

eprints@whiterose.ac.uk
https://eprints.whiterose.ac.uk/

Detonation shock dynamics of Type Ia supernovae

Scott D. Dunkley,[1]★ Gary J. Sharpe[1] and Sam A. E. G. Falle[2]

[1]*Department of Mechanical Engineering, University of Leeds, Leeds LS2 9JT, UK*
[2]*Department of Applied Mathematics, University of Leeds, Leeds LS2 9JT, UK*

ABSTRACT

The wavefront propagation of curved detonation waves in carbon–oxygen cores and helium shells of Type Ia supernova (SNIa) progenitors is determined via a detonation shock dynamics approach. A level set implementation is used to track the front, which is evolved according to intrinsic quasi-steady, quasi-one-dimensional detonation speed–curvature relationships. The effects of curvature are analysed for a number of SNIa models from the literature by comparing the results to those obtained by wavefront propagation at the local planar detonation speed. The differences can be very profound in the low-density regions where detonation models are exploited to produce intermediate-mass elements. In detonable low-density regions, the speed tends to be much lower than the planar wave analysis predicts, while the subsonic driving zone controlling the dynamics is many orders of magnitude shorter. However, the lower shock temperatures ensure that the complete reaction lengths are orders of magnitude longer when curvature effects are properly accounted. Furthermore, the material cannot be detonated in sufficiently low-density regions due to a curvature-induced extinction limit. The implications for and need to reassess the nucleosynthesis and intermediate-mass element production of SNIa detonation models is discussed.

Key words: nuclear reactions, nucleosynthesis, abundances – shock waves – supernovae: general – white dwarfs.

1 INTRODUCTION

It is currently accepted that Type Ia supernova (SNIa) originate from thermonuclear disruptions of carbon–oxygen (CO) white dwarfs, which may reach the Chandrasekhar mass via mass transfer from a companion. He (helium) accretes around the CO core, eventually resulting in the ignition of the core or shell (Hillebrandt & Niemeyer 2000). There are various modes of burning proposed to explain the resulting explosion. The main three candidates are detonation (supersonic burning), deflagration (subsonic burning) or delayed detonation models (a combination of both). The light curves and spectra of observed SNIa provide constraints on the prediction of models. The light curve is powered by the energy released due to ^{56}Ni as it radioactively β-decays to ^{56}Fe, ^{56}Ni $\rightarrow$^{56}Co $\rightarrow$^{56}Fe (Colgate & McKee 1969). About 0.5–$1.0\,M_\odot$ of ^{56}Ni needs to be produced in a model to agree with the observed light curves (Wheeler & Harkness 1990). A successful model would also produce the intermediate-mass elements Si, Ca, Mg, S and O as these are observed in the spectra at maximum light with a velocity range of 12 000–15 000 km s^{-1} (Branch et al. 1983).

Arnett (1969) was the first to compute a hydrodynamic simulation of a white dwarf in one dimension. He assumed a detonation as the burning mode and found expansion velocities up to 20 000 km s^{-1} and a significant amount of ^{56}Ni produced. While this satisfies the criteria that the model produces enough ^{56}Ni, pure detonation models of Chandrasekhar mass white dwarfs fail to satisfy the other criteria of high-velocity intermediate-mass elements in the outer layers. At the densities involved, the detonation burns the CO promptly to iron group elements. The density needs to be less than about 10^7 g cm^{-1} for a detonation to begin producing intermediate-mass elements as then the thickness of the detonation becomes comparable to the size of the star and hence burning can be incomplete (Khokhlov 1989). This is exploited in low-density sub-Chandrasekhar mass detonation models. The double-detonation model consists of a sub-Chandrasekhar CO core in which a detonation in the He envelope induces a detonation promptly at the core-envelope boundary (Nomoto 1982; Wiggins & Falle 1997), or subsequent to the detonation of the He envelope, the core centre (Woosley & Weaver 1994) or off-centre (Fink et al. 2010).

An alternative scenario to consider is a subsonic deflagration wave, which pre-expands the outer regions of a star. The delayed detonation model starts as a deflagration which pre-expands the star and then the explosion continues as a detonation in densities lower than 10^7 g cm^{-1}, leading to both intermediate-mass elements production and high velocities that give good agreement to the light curves and spectra (Khokhlov 1991). Plewa (2007) considers models in which a deflagration fails and some time later on, the remaining material detonates. It therefore seems that considering both delayed and double detonations, detonations may play an important role in SNIa.

★ E-mail: mnsdd@leeds.ac.uk

The simplest model of a detonation wave is a steady (in the wave's rest frame) and planar detonation (Fickett & Davis 1979). A self-sustaining wave of this form is known as Chapman–Jouget (CJ) if the flow is equilibrium sonic behind the wave. The CJ speed is the minimum possible speed in this case. However, the self-sustaining wave may travel faster than the CJ speed if endothermic effects are present. In this case, the wave is known as a pathological detonation and the sonic point is inside the reaction zone. Khokhlov (1989) investigated the speed and structure of a steady planar detonation in CO. The structure was shown to consist of three distinct stages: a carbon (C) burning stage, then an oxygen (O) burning stage and finally a silicon (Si) burning stage. The C burning stage is the shortest, being an order of magnitude or more smaller than the O burning stage, itself orders of magnitude shorter than the Si burning stage. Khokhlov (1989) also found that nuclear detonation waves in CO are of the pathological type for densities greater than about 2×10^7 g cm^{-3}. In these cases, the sonic point occurs at the end of the O burning stage due to endothermic Si burning, but he did not determine the complete structure due to the singular nature of the sonic point and hence instead considered only supported (or over-driven) detonation waves. Sharpe (1999) subsequently determined the self-sustaining wave structure for these densities, revealing that the length-scales of the pathological detonations are a few times thicker than their supported equivalents.

Since detonation waves result from a point ignition in SNIa scenarios, the expanding wavefront will be intrinsically curved. Sharpe (2001) investigated the effects of curvature on CO detonation speed and wave structure. He determined the normal detonation speed–curvature ($D_n-\kappa$) relation for various densities and concluded that taking curvature properly into account might profoundly alter the outcome of low-density SNIa explosion models. For high densities, the response to curvature is found to be similar to detonations with temperature sensitive simple reaction networks (Stewart 1998; Sharpe 2000a,b), whereby increasing the curvature reduces the detonation speed by only a couple of per cent before a critical or extinction curvature is reached. The detonation cannot propagate when the shock front curvature becomes higher than this value, as the shock temperature then becomes too low to ignite the reactions. This results in the failure of the wave with the reaction zone decoupling as the shock decays to an acoustic wave (Stewart & Yao 1998).

For lower CO densities, the $D_n-\kappa$ relation becomes multi-branched (Sharpe 2001; Messoudi, Vidal & Busegnies 2009). In these cases, very small increases of curvature result in the detonation speed dropping rapidly from the planar value. A further increase in curvature results in a step change in the speed as the sonic point jumps from the end of Si burning to that of O burning. The dynamics are then controlled by the much shorter C and O burning stages, while Si burning occurs in a supersonic region which cannot communicate with the front. Messoudi et al. (2009) identified a third branch as the curvature increases further, associated with the sonic point jumping to the end of C burning and a further step drop in detonation speed. Extinction of the detonation can only occur once the curvature is sufficiently high to extinguish the C burning for these cases. When the curvature becomes sufficient for the detonation to be driven only by C and/or O burning, due to much lower detonation speeds and hence shock temperatures, the Si burning length becomes orders of magnitude longer than the planar structure predicts. While this is immaterial to the front dynamics because it occurs beyond the sonic point, it has profound implication for nucleosynthesis and production of intermediate-mass elements. While relaxing the planar assumption, the $D_n-\kappa$ analysis assumes quasi-

one-dimensional, quasi-steady evolution. If the subsonic driving zone of the reactions become comparable to any other length-scale in the problem, then time-dependence also needs to be accounted for and any steady or quasi-steady models break down. For SNIa, other problem length-scales include the radius of the CO core (of the order of 10^8 cm) and the density scaleheight.

Due to the highly multiscale nature of the problem (from less than 1 cm for C burning to over 10^8 cm for the size of the star), a fully resolved numerical simulation of the detonation events throughout the entire star is essentially impossible. It is important to note that only in the specific case of planar, steady and CJ detonations that jump conditions across the wave can be applied, allowing the wave to be 'captured' (unresolved) in numerical simulations. In any other case (pathological detonations, curved detonations, time-dependence in the reaction zone), the dynamics and wave structure are non-linearly coupled and one must fully resolve the driving part of the reaction zone to compute the solution (Aslam, Bdzil & Hill 1998; Sharpe & Braithwaite 2005; Bdzil & Stewart 2007). Since the driving zone part of the structure determines the dynamics, if this occurs on scales which are not large compared to the available grid spacing, then this requires a subgrid model to properly resolve this zone.

Several attempts have been made at such subgrid modelling of SNIa detonations by assuming the detonation propagates at the planar detonation speed which depends only on the local density ahead of the wave. Wiggins & Falle (1997) have investigated the double-detonation models of Nomoto (1982) in two dimensions using the method of geometrical optics. However, the planar speed assumption is only consistent with the steady planar limit. One or both of these assumptions must in fact break down for the low-density regions where detonations can be exploited to produce intermediate-mass elements via incomplete Si burning. Either curvature must drive the sonic point to the end of O burning, so that the incomplete burning occurs after the subsonic driving zone, or else the wave must be intrinsically unsteady due to the incomplete reactions.

Very similar issues to those described above arise in engineering applications of so-called non-ideal explosives, which has led to the development of a set of subgrid models collectively known as 'detonation shock dynamics' (DSD) (Stewart 1998; Bdzil & Stewart 2007). DSD exploits the $D_n-\kappa$ and higher order theories to precompute the wave dynamics under the action of front curvature.

Despite the profound effect of curvature on low-density CO (Sharpe 2001; Messoudi et al. 2009), to date no attempt has been made to apply DSD to SNIa. Fink et al. (2010) present some preliminary results of a novel, but ad hoc, iterative method for taking into account incomplete burning. Townsley et al. (2009) employ a simple three-stage nuclear reaction mechanism. Even with a reduced mechanism, a subgrid model will still be required for the first and second reactions (representing C and O burning) due to the disparity in length-scales with the star size. Furthermore, such reduced models may have quite different curved detonation dynamics than that predicted by detailed nuclear reaction models, unless they are calibrated. The purpose of this paper is to develop and apply DSD subgrid models for computing detonation in full star SNIa simulations using the intrinsic $D_n-\kappa$ relationships for CO and He. The predictions of the DSD calculations are compared to those assuming planar detonation speeds for a number of representative detonation models in the literature.

The DSD methods employed in this paper are not 'ad hoc', but based on rigorous analyses of the full reactive compressible flow. These analyses in particular show that the balance of heat release with the nozzling effect due to shock front curvature results in a

part of the reaction zone as well the subsequent expansion of burnt products of detonation being supersonic with respect to the shock front. It is precisely this decoupling of scales that allows one to formally construct solutions of the driving zone part of the detonation and hence to pre-compute the front propagation, independent of the following flow.

It is to be stressed out from the outset that in this paper we are concerned only with the 'inner' detonation dynamics aspects of the problem. The details of the larger scale hydrodynamic evolution of the supersonic part of the flow will be considered in a sequel, although a number of implications for this 'outer' region are discussed based on the DSD results. Nevertheless, it should be noted that the detonation speeds, driving zone structures and corresponding partially burnt sonic 'exit' states integral to the DSD part of the solution are determined from detailed and highly resolved calculations of the fully coupled reactive flow (Sharpe 2001).

The only approximation to the entire solution of the problem in the presented results is that we have assumed the leading-order DSD solution in order to obtain the speeds and driving structures. This approximation is equivalent to assuming, within the driving zone only, that the driving zone length remains small both with respect to the radius of curvature of the shock and to any other length-scales in the problem or that the transit time for a particle to traverse the driving zone is short compared to the time-scales of changes of the detonation speed and structure. The detonation speed (by which the characteristic time-scale can be determined given the driving zone length) is only a weak function of density or radius in SNIa; at this order of approximation, these two statements may be considered equivalent.

Indeed, transverse effects and weak time-dependence typically arise at the same higher order in DSD theories (Bdzil & Aslam 2000). Nevertheless, the validity of the quasi-one-dimensional (and hence quasi-steady) approximation can be checked for self-consistency by comparing the local length-scales of the computed DSD solution at every point in the star with the other length-scales which arise in the problem, and we do this throughout. In fact, provided this approximation is only violated in localized regions, this should not have a large effect on the validity of the global solution, due to the fact that the DSD solutions represent the stable attractors of the system. In other words, highly transient regions tend to rapidly asymptote back to the quasi-steady DSD solutions.

2 DETONATIONS IN SNIA

In this section, the characteristic properties of detonations in CO core and He shells are briefly summarized. The results presented here employed an α-network for the nuclear reactions, consisting of 13 species linked by 27 reactions with the reaction rates taken from Fryxell et al. (1989) and an equation of state with contributions from radiation, non-degenerate ions and arbitrarily degenerate and relativistic electrons and electron–positron pairs (Sharpe 2001). Messoudi et al. (2009) have shown that a full nuclear reaction of 331 species predicts the same qualitative trends in the detonation speeds as the α-network (albeit at a very significant increase in computational cost), but can result in quantitative differences in extinction curvatures and detonation speeds. We stress however that the purpose here is to examine the large *qualitative* differences in front propagation when curvature effects are included, for which the α-network is sufficient. The *quantitative* changes induced by incorporating a complete nuclear reaction network will be addressed in a sequel. The methodology for determining the $D_n - \kappa$ relations is described in Sharpe (2001). Throughout, an initial temperature of

10^8 K assumed and an initial composition of the core to be 0.5 C and 0.5 O have been assumed.

2.1 Planar and steady detonations

The planar detonation speed, D_{planar}, as a function of initial density (i.e. corresponding to the local density just ahead of the shock front) for both CO and He can be seen in Fig. 1(a). For densities between 3×10^6 and 2×10^7 g cm^{-3}, the CO detonation speed drops as Si burning produces less energy due to the equilibrium composition becoming enriched with light and intermediate-mass elements (Gamezo et al. 1999). For densities higher than this, the wave is of the pathological type with endothermic Si burning taking place such that the sonic point is located at the end of O burning (Sharpe 1999). The planar detonation speed in He is higher than that in CO. The dependence of the reaction zone length-scales, l_{planar} (i.e. the distance between the shock and the sonic point for a planar detonation) on initial density is also shown for both materials in Fig. 1(b). The CO detonation length is longer than that in He for a given initial density. However, the length-scales can be seen to increase by orders of magnitude as the density drops. The detonation length becomes comparable to the size of the star (10^8 cm) at $\rho_0 = 10^7$ and 6×10^6 g cm^{-3} for CO and He, respectively. For pathological CO detonations at higher densities, the effective reaction lengths (distance between the sonic point and the shock) is shown and hence a
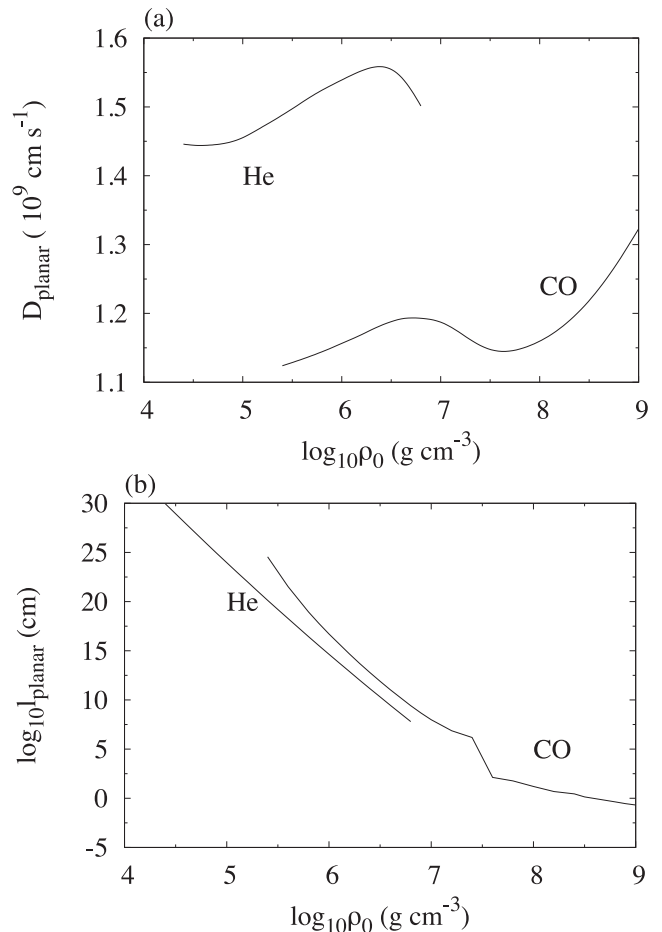

Figure 1. (a) Speed and (b) distance between the shock and sonic point for planar detonations as functions of initial density for CO and He.

rapid drop in length occurs at $\rho_o = 2 \times 10^7$ g cm^{-3} due to the jump in the sonic point position (Fig. 1b).

2.2 $D_n - \kappa$ relations

Fig. 2 shows the normal detonation speed response to curvature in CO for a variety of initial densities. The dashed line represents the full solution curves of the quasi-one-dimensional, quasi-steady equations (Sharpe 2001). However, only the stable branches with
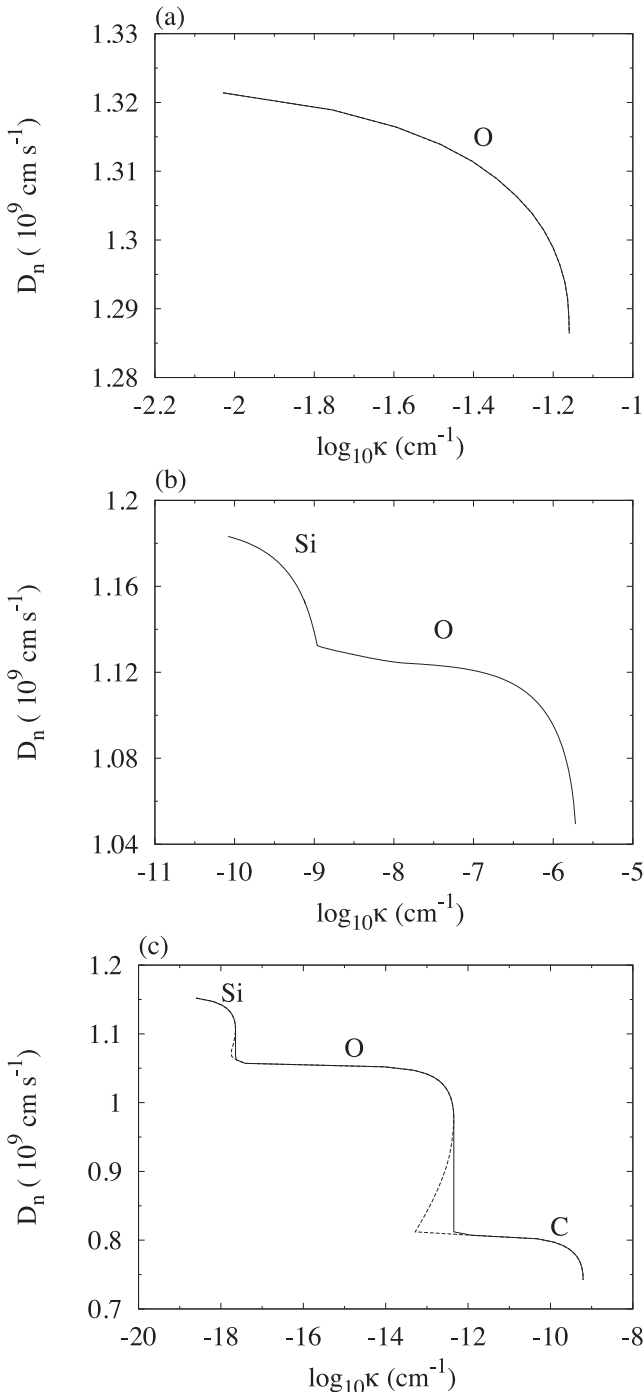
Figure 2. $D_n - \kappa$ curves for curved CO detonations and initial CO densities (a) 10^9, (b) 10^7 and (c) 10^6 g cm^{-3}. The solid line indicates the evolution path of an expanding front.

negative slope are physically relevant and hence the solid lines show the evolutionary path corresponding to an expanding detonation front. For high densities, the detonation speed does not drop very much (e.g. only by ∼3 per cent for a density of 10^9 g cm^{-3}, Fig. 2a) before the extinction curvature is reached (corresponding to a turning point in the $D_n - \kappa$ curves). As discussed above, at these densities the planar ($\kappa = 0$) wave is pathological and the sonic point remains near the end of O burning up to extinction. For the low initial densities of interest here, the $D_n - \kappa$ curves are multibranched (e.g. Figs 2b and c, corresponding to densities of 10^7 and 10^6 g cm^{-3}, respectively). The high-speed branch (labelled Si in Figs 2b and c) corresponds to very weakly curved (near CJ) detonation propagation with the isolating sonic point occurring near the end of Si burning, the middle branch (labelled O) corresponds to detonation driven only by C and O burning and the low-speed branch corresponds to the subsonic driving zone consisting only of the C burning stage. Each of these branches may have its own extinction point, beyond which the solution switches to the next branch. Only when the extinction of the low-speed branch is reached, does the curvature induce complete detonation failure. Thus in low densities, detonation speeds much lower than the CJ value can be sustained, as can detonation fronts with very high curvatures based on the CJ length-scale.

The transition between branches as the wave evolves cannot of course occur instantaneously in the full problem, i.e. these transitions are dynamic events and hence would occur over some timescale. However, the existence of the branch extinction and transitions are due to extreme sensitivity of autoignition times on the shock speed (and hence shock temperature), such that these transitions usually occur via self-accelerating shock–reaction zone coupling or decoupling effects and hence tend to be rapid. For example, experimental and numerical results show that curvature-induced failure occurs as a very fast decoupling of the shock and reaction zone, leading to a 'sudden death' of the shock-induced chemistry and rapid decay of the shock to an acoustic wave (Radulescu et al. in preparation). Thus in this paper, to a first approximation, the transitions between solution branches are treated as instantaneous jumps on the time-scales of interest.

Fig. 3 shows the distance between the shock and the sonic point, l, in a CO detonation as a function of curvature for the three initial densities 10^6, 10^7 and 10^9 g cm^{-3}. Due to the jump in the location of the isolating sonic point from the end of Si burning to the end of O burning to the end of C burning with increasing curvature, the driving zone reaction lengths on the different branches are typically orders of magnitude different on these branches.

Fig. 4(a) shows the value of the extinction curvature of each branch as a function of initial density. The higher the initial density, the larger the curvature required for the detonation to fail due to the rapidly decreasing reaction length-scales. For densities less than 1.11×10^7 g cm^{-3}, the detonation only fails when the C branch extinction curvature is reached. For a point initiated detonation propagating through a CO core, one would in general expect the radius of curvature of the shock front to be of the order of the CO radius or of the density scaleheight (both ∼10^8 cm for the cases considered) or less, corresponding to curvatures of the order of 10^{-8} cm^{-1} or more. However, Fig. 4(a) shows that for densities less than about 1.8×10^6 g cm^{-3}, the detonation will be extinguished whenever such curvatures are encountered. Hence, it would be unlikely that a detonation could be established or maintained in CO regions where the density is less than this and clearly this has important implications for SNIa detonation models involving very low density regions.
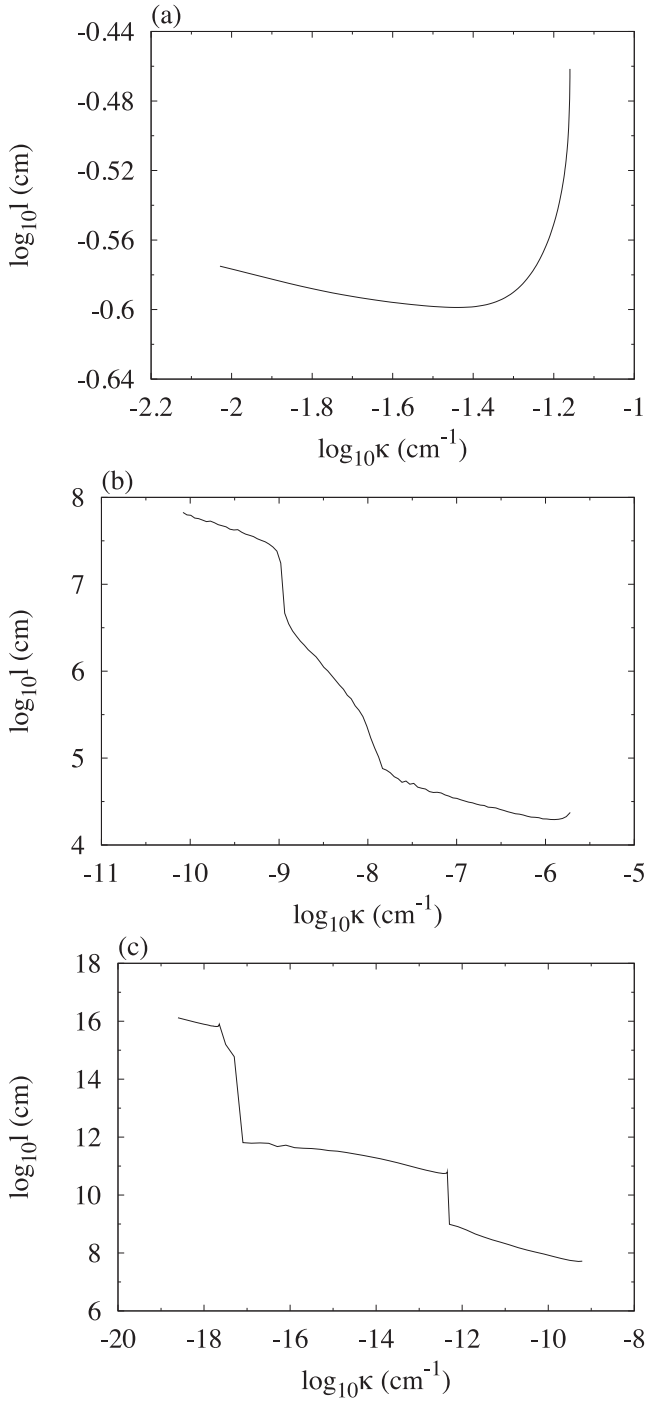
Figure 3. Driving zone reaction lengths (distance from shock to the sonic point) for curved CO detonations as a function of shock front curvature, for initial densities of (a) 10^9, (b) 10^7 and (c) 10^6 g cm^{-3}.

Figure 4. (a) Extinction curvature, (b) D_n/D_{planar} and (c) driving reaction length (distance from shock to the sonic point) at the turning point of each $D_n - \kappa$ solution branch for curved CO detonations, as a function of initial density.

Fig. 4(b) shows the detonation speed at the turning point relative to the corresponding planar speed, D_n/D_{planar}, attained at the turning points of the three branches. The difference in detonation speed between the O and C branches is greater than from the Si to O branches. Therefore when the sonic point drops to the C branch, one would expect curvature effects to be their greatest in comparison to the planar propagation.

Finally, Fig. 4(c) shows the driving zone reaction lengths for each branch as measured at the turning point. The Si branch reaction
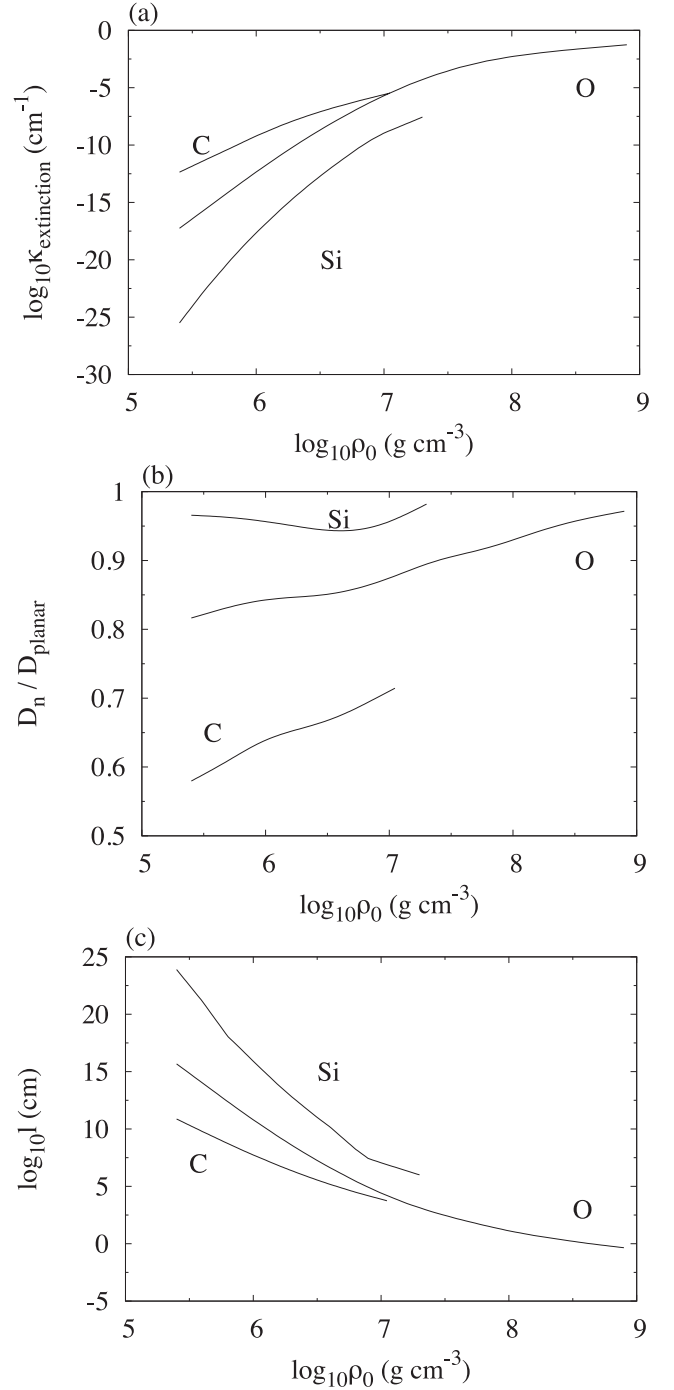
lengths are the largest and if the sonic point is located here, the reaction length would be comparable or larger than the core radius or the density scaleheight. At a density of about 6.75×10^6 g cm^{-3} the reaction length is already 10^8 cm. Therefore, as the turning point is approached on the Si branch, the quasi-one-dimensional, quasi-steady assumptions of the $D_n - \kappa$ analysis begins to break down. The driving lengths of the O branches are orders of magnitudes smaller than on the Si branch and those of the C branch much smaller still. Hence, the assumptions of the $D_n - \kappa$ theory is more self-consistent
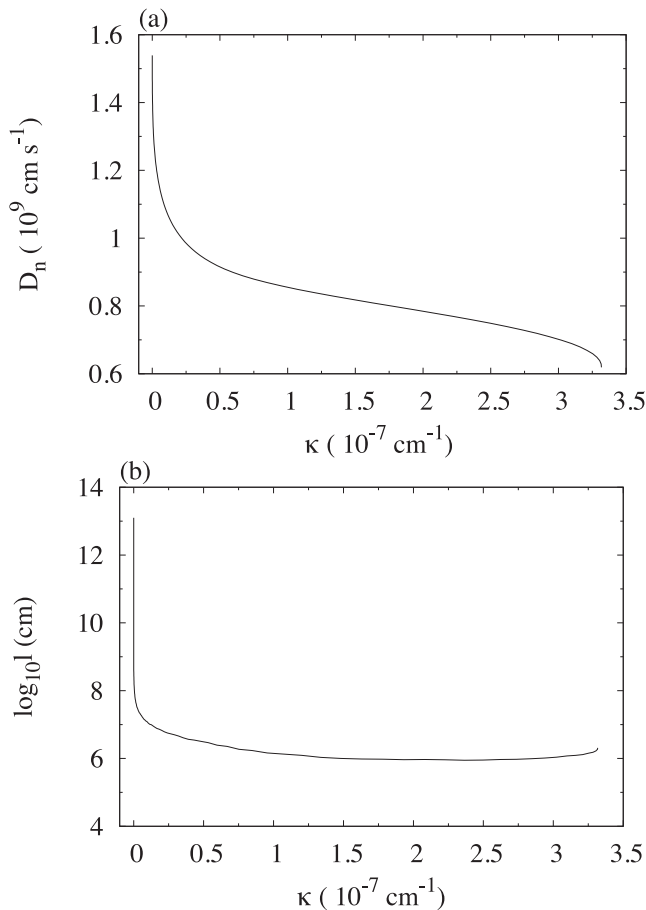
Figure 5. (a) $D_n-\kappa$ curve and (b) corresponding driving reaction length (distance from shock to sonic point) for curved He detonations with initial density 10^6 g cm^{-3}.

for propagation on these branches. However, these lengths begin to increase rapidly as the turning point of a branch is approached. Even the C branch will have reaction lengths larger than the core radius for low enough densities (less than about 8.8×10^5 g cm^{-3}) near its turning point. Hence, when applying DSD to SNIa explosions, it will be important to check whether the results are consistent with the slowly varying assumptions of the theory.

Khokhlov (1989) also discusses the wave structure for He burning. For densities $\geq 5 \times 10^6$ g cm^{-3}, He burns directly to Ni with very little intermediate-mass element production within the wave structure. At densities below this, a thermally neutral relaxation layer follows the burning layer, increasing in thickness with decreasing density. The $D_n-\kappa$ curves for He are found to consist only of a single branch at all densities (Dunkley, Sharpe & Falle, in preparation). Fig. 5(a) shows a typical $D_n-\kappa$ curve for He, corresponding to an initial density of 10^6 g cm^{-3} (the results for other densities are found to be qualitatively similar – the effects of curvature on He detonation are to be discussed in detail in a paper in preparation). Fig. 6(a) shows the extinction curvature of the He detonations as a function of initial density. Lower densities have smaller extinction curvatures due to increasing reaction lengths. Again in SNIa, detonation fronts with radii of curvatures greater than the characteristic size of the star or density scaleheight are unlikely to be encountered. For He, the extinction curvature is less than 10^{-8} cm^{-1} in regions where the density is less than about 2×10^5 g cm^{-3}. Thus, a detonation would not propagate very far into such a low density before
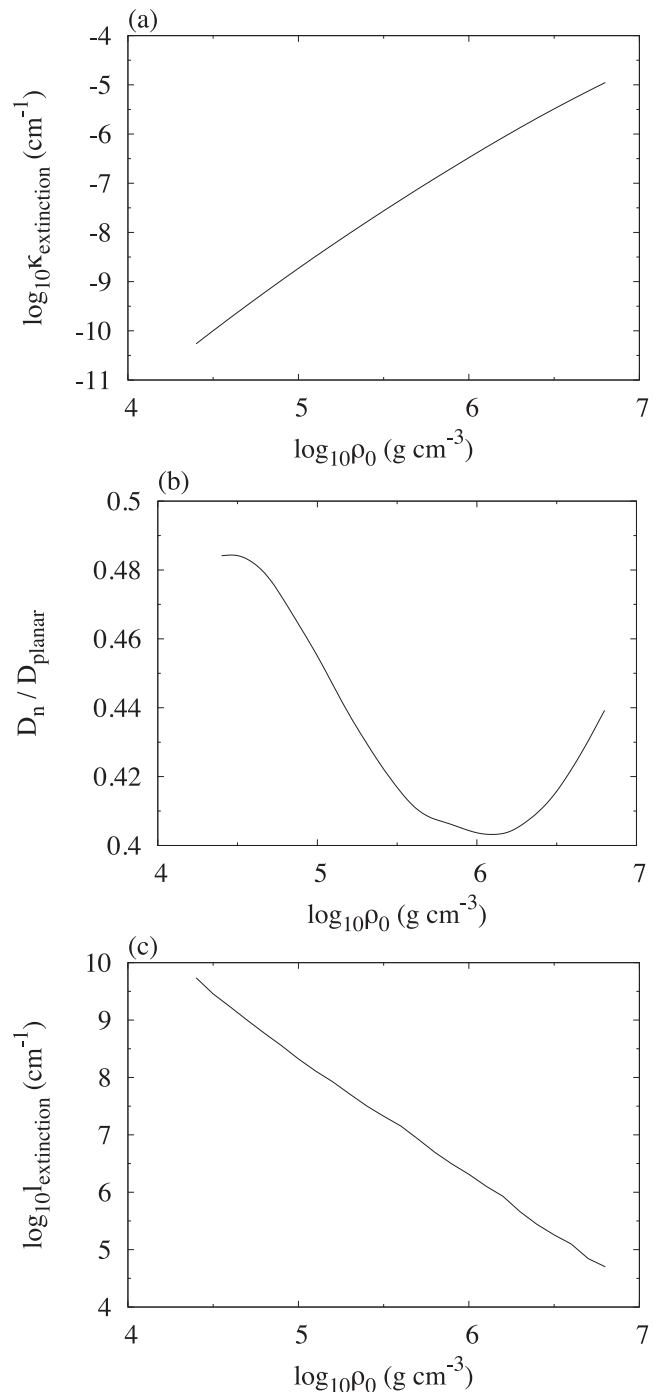

Figure 6. (a) Extinction curvatures, (b) D_n/D_{planar} and (c) driving reaction length (distance from shock to the sonic point) at the turning point of the $D_n-\kappa$ solution for curved He detonations, as a function of initial density.

becoming extinguished and again this has important implications for SNIa models involving detonation of low density He shells. However, Fig. 6(b) shows that detonations can be sustained in He with larger velocity drops from the planar value compared to those in CO. Indeed, the speeds at the extinction point in Fig. 6(b) are all below half that of their planar value. The driving reaction lengths of He also increase rapidly as the density decreases (Fig. 6c). The driving length at the extinction point becomes larger than 10^8 cm at a density of 1.5×10^5 g cm^{-3} and hence again it will be necessary

to check the validity of DSD theory when applied to SNIa in regions with densities lower than this.

3 LEVEL SET METHOD IMPLEMENTATION

To investigate the effects of curvature on the front dynamics of detonations in SNIa, we employ level set methods to compute the propagation of the front. A general discussion of such methods is given by Sethian (1999) and the implementation for curved detonations is described by Aslam, Bdzil & Stewart (1996). To summarize briefly, the level set method involves embedding a surface of interest (the detonation front in this case) in a field one dimension higher. This field, ψ, is then evolved and the surface of interest within this field evolves accordingly, handling convergence, divergence, etc. of the evolving front automatically. We identify the level curve $\psi = 0$ with the detonation front, such that $\psi > 0$ and $\psi < 0$ correspond to the unburnt and burnt material, respectively. The location of the front can then be determined at any time by standard contouring routines or instead a burn table can be constructed (Aslam et al. 1996) in which the time is recorded when the $\psi = 0$ level set passes through a computational cell.

In this paper, two-dimensional axisymmetric calculations are performed with cylindrical (r, z) coordinate system and the level set equation is

$$\frac{\partial \psi}{\partial t} + D_n(\rho_0, \kappa) |\nabla \psi| = 0. \tag{1}$$

where

$$\kappa = \frac{\psi_{rr}\psi_z^2 - 2\psi_r\psi_{rz}\psi_z + \psi_r^2\psi_{zz}}{\left(\psi_r^2 + \psi_z^2\right)^{3/2}} + \frac{\psi_r}{r\sqrt{\psi_r^2 + \psi_z^2}}. \tag{2}$$

This differs from that in Aslam et al. (1996) due to the extra geometric curvature term. Note that this definition of curvature corresponds to the mean curvature as it appears in the DSD equations. However, the numerical scheme used is otherwise similar. It is important to note $D_n(\rho_0, \kappa) = D_{\text{planar}}(\rho_o) - \alpha(\rho_o, \kappa)$ and hence both the hyperbolic (first term) and parabolic (second term) parts (Sethian 1999) are spatially varying.

There are two types of boundary conditions relevant to our problem. These are symmetric (perfectly reflecting) and non-reflecting (inflow/outflow). The second-order scheme requires two levels of ghost nodes per boundary. At the end of each time step calculation, for the symmetric boundary condition the two interior nodes nearest to the boundary are simply reflected to the exterior, e.g. $\psi_{-2,j}^n = \psi_{2,j}^n$ and $\psi_{-1,j}^n = \psi_{1,j}^n$ for $\psi_{0,j}^n$ at $\psi_{0,j}^n = 0$. Quadratic extrapolation is used for the non-reflecting condition, or equivalently, imposing that the second derivative is constant along the normal on the boundary, e.g. $\psi_{-1,j}^n = 3\psi_{0,j}^n - 3\psi_{1,j}^n + \psi_{2,j}^n$. The symmetry boundary condition is employed on the axis $r = 0$, while the non-reflecting boundary conditions are employed on all other boundaries.

The initial conditions consists of a spherical detonation with a small radius, e.g. arising from a localized ignition event and ψ is initialized according to

$$\psi(r, z, t = 0) = \sqrt{(r - r_1)^2 + (z - z_1)^2} - R_0. \tag{3}$$

Thus, the initial front has a radius R_0 centred on the point (r_1, z_1) and the initial level set field is hence the signed distance function from this.

Finally, it should be noted that while in this paper we only consider one-dimensional (spherically symmetric) and two-dimensional (axisymmetric, single point initiation) SNIa scenarios

from the literature, DSD methods and their level set implementations are specifically constructed to be readily extendible to three dimensions and to naturally account for multiple wavefronts from multiple initiation sources, the interactions and merging of disconnected fronts, etc. (Bdzil & Stewart 2007). More complex geometries will hence be considered in a sequel.

4 APPLICATION AND RESULTS

In this section, we apply the front propagation algorithms to various SNIa detonation scenarios in the literature. In each case, the front dynamics are computed first by assuming that the detonation propagates at the local planar detonation speed as in Wiggins & Falle (1997). Henceforth, we refer to this as the planar detonation speed (PDS) model. This is then compared with DSD propagation according to the $D_n - \kappa$ assumptions (referred to as the DSD model). The purpose here is to investigate the qualitative changes in the predictions of SNIa detonation models when curvature effects are taken in to account.

4.1 Spherically symmetric models

We begin by investigating one of the one-dimensional (spherically symmetric) models of Woosley & Weaver (1994). They discuss a case (referred to as Model 2 in their paper) in particular detail. Model 2 consists of a $0.7\,M_\odot$ white dwarf that accretes $0.2\,M_\odot$ of He. A He detonation starts at the base of the accreted He ($r = 4.03 \times 10^8$ cm, $\log_{10}\rho_0 = 6.28$ g cm^{-3}) and propagates outwards. In this model, the He detonation is initiated simultaneously at every point of the base in the He shell. The He detonation also results in an inert shock which travels inwards towards the core, compressing the CO matter. This inert shock then ignites the CO at the centre where the shock front converges, resulting in a CO detonation propagating outwards.

In the spherically symmetric case, the shock radius R_s is related to the detonation speed D_n in the shock normal (radial) direction n by

$$\frac{dR_s}{dn} = D_n(\rho_0, \kappa), \tag{4}$$

while the front curvature is simply $\kappa = 2/R_s$ [for the PDS case the detonation speed is simply $D_{\text{planar}}(\rho_0)$]. Equation (4) is solved by numerical integration. Given the shock position, the density is determined from the density profile in Woosley & Weaver (1994) (Fig. 7).

Fig 8 shows the results of the first-stage He detonation, consisting of the detonation shock radius as a function of time (Fig. 8a) and the corresponding detonation speed evolution (Fig. 8b) for both the PDS and DSD theories. As the detonation progresses outwards, despite the decreasing curvature of the shock (increasing R_s), the rapidly increasing effect of curvature, as lower densities are encountered ahead of the detonation, results in the detonation speed dropping significantly more for the DSD than the PDS. The DSD and PDS solutions thus diverge as the front propagates outwards. For the PDS model, one must take the reaction zone length to be that of the planar detonation, in order to be consistent with the underlying assumption of propagation at the planar detonation speed. However, for Model 2, the corresponding He detonation reaction lengths are then always orders of magnitude greater than the stellar radius (6×10^8 cm) or density scaleheight (of the order of 10^8cm). Hence, this is a first example of where the planar speed assumption is self-inconsistent. In this case, the reactions could not be completed in
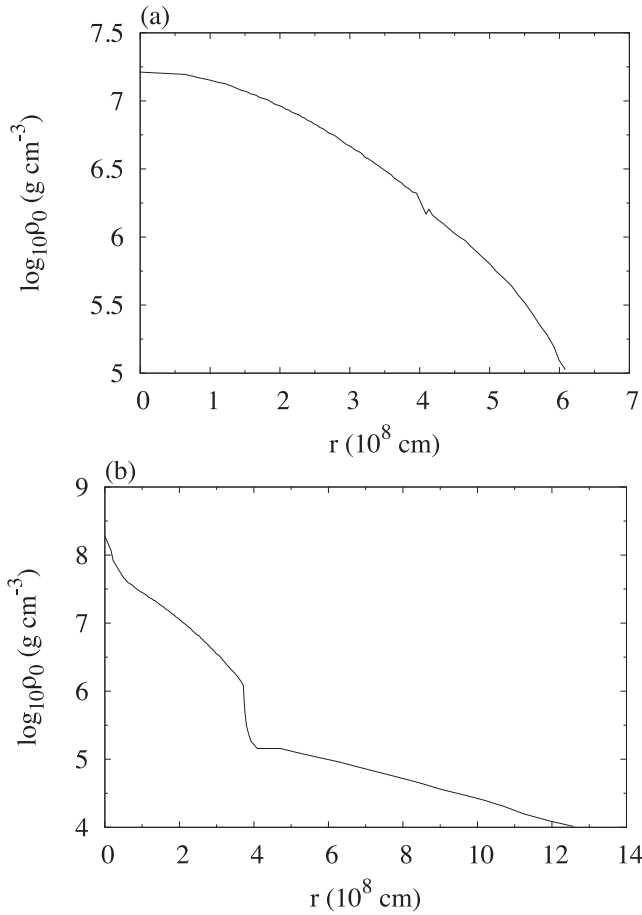
Figure 7. Density profiles for Woosley and Weaver's Model 2: (a) prior to ignition of the first stage off-centre He detonation and (b) at the time of central ignition of the second-stage CO detonation.

Figure 8. (a) Detonation time and (b) detonation speed as functions of shock radius for the He detonation stage of Model 2 of Woosley & Weaver (1994).

the time-scale of the explosion since the required length-scales are larger than the star, but the planar speed assumption necessitates complete burning. However, note that the quasi-steady, quasi-one-dimensional assumptions of DSD are entirely self-consistent in this case. The shock front curvature affects the sonic point significantly, driving it inwards, so that the subsonic driving zone becomes an order of magnitude or more smaller than any other length-scale of the problem. The detonation front is extinguished at $R_s = 5.99 \times 10^8$ cm ($\log_{10}\rho_0 = 5.1$ g cm^{-3}).

For the second stage of Model 2, we follow the CO detonation from ignition at the centre up to where the CO ends and the burnt products of the He detonation starts at $r = 3.72 \times 10^8$ cm (Fig. 7b, here $t = 0$ s is now the time of central ignition). Note that in such two-stage detonation scenarios, the conditions up to the point of detonation ignition of the CO core are created by a hydrodynamic evolution induced by the He detonation stage. However, since the detonation propagation is very high for most of its propagation time in the core (i.e. Mach number of the order of $\backsim$5), the hydrodynamics state ahead of the detonation can be considered to be frozen (e.g. Fig. 7). Furthermore, the flow velocities ahead of the front are always at least an order of magnitude less than the detonation speed so that again this effect can be neglected to leading order. Fig. 9 shows the evolution of the shock radius and the detonation speed for this stage. Near the centre the density is relatively high and curvature effects are not significant; hence, initially the PDS and DSD models give similar results. The sonic point is at the end of oxygen
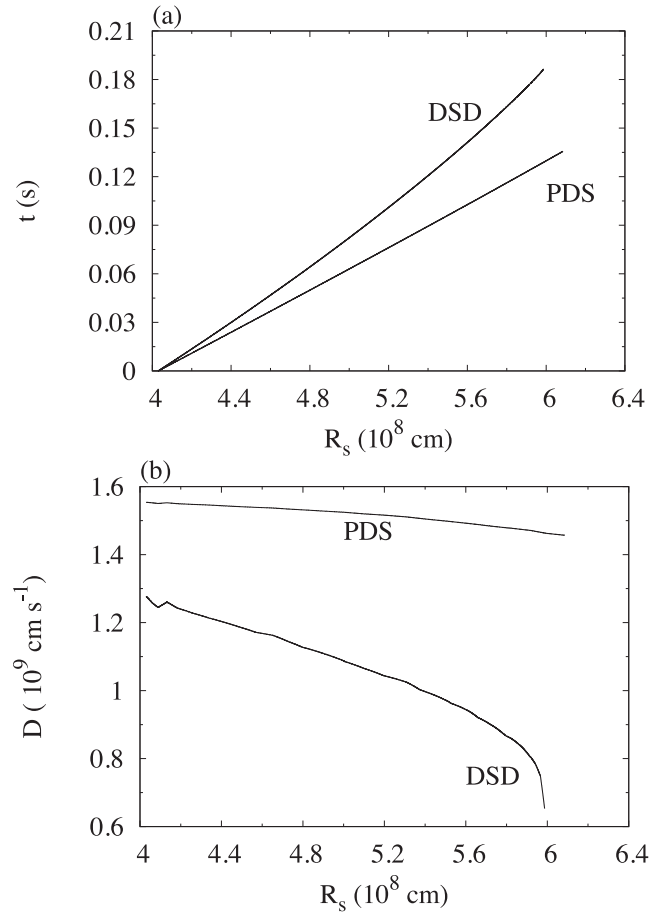
burning (i.e. on the O branch) due to the wave being pathological. At 0.11 s ($R_s = 1.41 \times 10^8$ cm, $\log_{10}\rho_0 = 7.30$ g cm^{-3}), the density and curvature are such that the sonic point jumps to the end of Si. However, this is only a brief period. The sonic point transitions back to the O branch solution at 0.12 s ($R_s = 1.63 \times 10^8$ cm, $\log_{10}\rho_0 = 7.21$ g cm^{-3}) as curvature effects become more important. The detonation speed in DSD becomes noticeably less than that of the PDS since the PDS sonic point then remains at the end of silicon burning. The turning point of the O branch is subsequently reached at 0.24 s ($R_s = 2.95 \times 10^8$ cm, $\log_{10}\rho_0 = 6.58$ g cm^{-3}), beyond which the solution drops down to the branch corresponding to the sonic point at the end of C burning. The DSD version does not reach the interface of the CO with the burnt products of the first stage. The curvature-induced detonation extinction point corresponding to the turning point of the C branch is encountered just before the arrival at the interface at 0.32 s ($R_s = 3.58 \times 10^8$ cm, $\log_{10}\rho_0 = 6.20$ g cm^{-3}). As there is no extinction mechanism in the PDS model, this erroneously predicts that the whole of the CO core would be completely detonated. In fact, the PDS model becomes inconsistent at around 0.18 s ($R_s = 2.3 \times 10^8$ cm, $\log_{10}\rho_0 = 6.9$ g cm^{-3}), due to the planar detonation reaction length-scales required for complete burning under the PDS assumption becoming greater than the size of the core and the density scaleheight. The DSD model remains more self-consistent, however, since curvature induces the driving zone length to remain smaller than these scales. The maximum value the driving zone length attains is 6.2×10^6 cm, located just
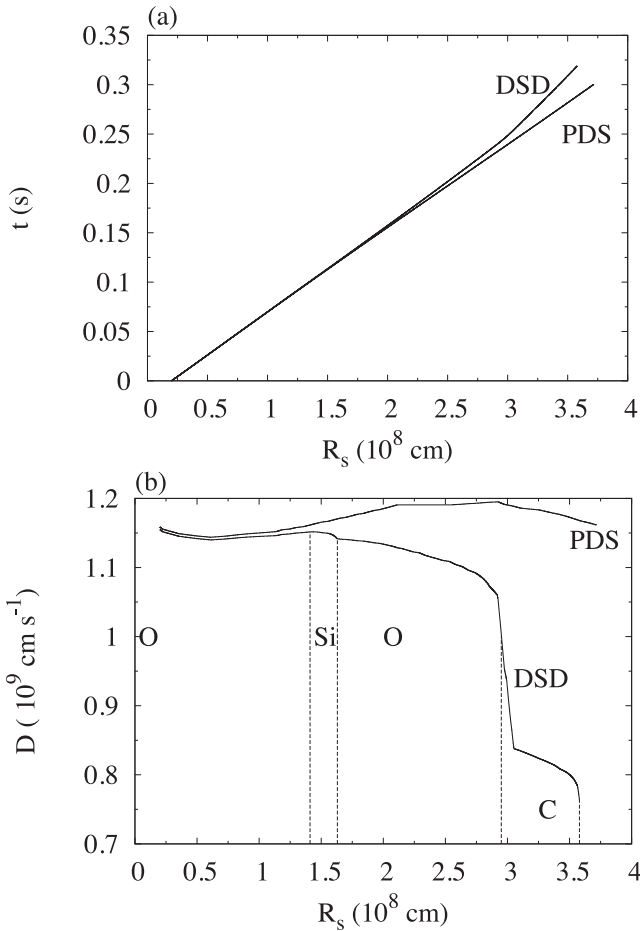
Figure 9. (a) Detonation time and (b) detonation speed as functions of shock radius for the CO detonation stage of Model 2 of Woosley & Weaver (1994). DSD regimes of propagation are marked by dashed lines in (b), where Si, O and C refer to the $D_n - \kappa$ solution branch in CO.

before the front is extinguished, which is far below the value of the core radius.

4.2 Off-centre models

In this section, the effects of curvature on representative two-dimensional (axis-symmetric) models from the literature are investigated.

4.2.1 Case A

The first model to be considered is a double-detonation model originally investigated as a one-dimensional spherically symmetric model (Case A) by Nomoto (1982). Case A experiences an explosion due to a He shell flash when a substantial amount of He has accreted on to the white dwarf. Fig. 10 shows the density profile of the white dwarf at the time of ignition. Nomoto (1982) investigates the results of this flash and finds that it produces a detonation wave at the base of the He envelope, consisting of a He detonation propagating outwards, which, unlike Model 2 of Woosley & Weaver (1994) above, simultaneously drives a detonation wave in the CO core. A two-dimensional version of Case A, corresponding to a point ignition source rather than ignition of the entire base of the shell was subsequently investigated by Wiggins & Falle
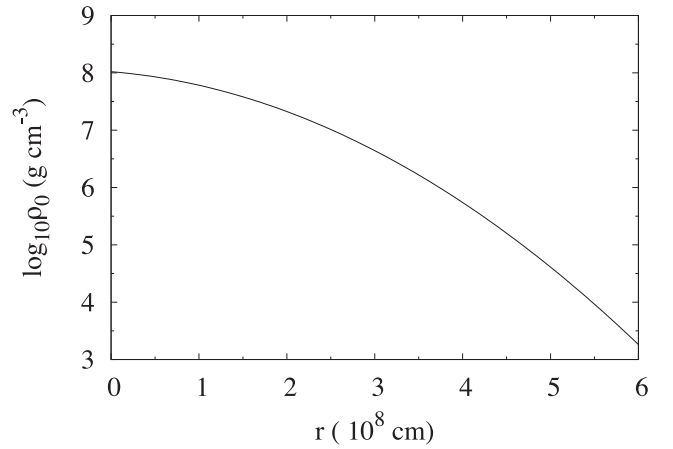

Figure 10. Density profile for Case A.

(1997), who used geometric optics to pre-compute the evolution of the detonation waves under the PDS assumption. The detonation is ignited at $r = 3.17 \times 10^8$ cm, just above the interface at $r = 3.14 \times 10^8$ cm, in this case. They found that two cusps form on the wavefront in the core due to the faster driving He detonation and suggest that these cusps may have important implications for nucleosynthesis.

Fig. 11(a) shows the level set evolution of the double-detonation Case A model for the PDS assumption. This is similar to the geometric optics construction results of Wiggins & Falle (1997), i.e. in which the detonation wave front has two cusps. The outer cusp is on the interface and is due to the faster He detonation than in the CO. The other is interior to the core and is a consequence of the dependence of the planar detonation speed on the local density. It takes 0.51 s for the CO core to be completely detonated. Fig. 11(b) shows the DSD version of the evolution when curvature effects are taken in to account. When the front speed depends on curvature, sharp cusps or corners cannot form due to the parabolic (smoothing) effect of the curvature term (Sethian 1999). Hence, one qualitative difference is that, unlike for the PDS model, the cusps are smoothed out in the DSD evolution. Furthermore, the curved detonation speeds in the relatively low density He shell are significantly below the planar values; hence, the He detonation's driving effect is not as strong compared to the planar case. Indeed, the curvature is sufficiently high in the outer parts (above a radius of about 4.4×10^8 cm, corresponding to $\log_{10}\rho_o = 5.32$ g cm^{-3}) of the He shell to extinguish the detonation completely.

Fig. 11(c) shows the $D_n - \kappa$ solution branch on which the detonation front propagates as it passes through each point. In the inner regions of the core nearer the centre the detonation travels close to the planar configuration due to the relatively high densities. Since for these densities the planar wave is pathological, here the solution evolves on the O branch (sonic point near the end of oxygen burning). Further out from the centre of the star, there is a narrow region around the centre corresponding to the planar wave solution becoming near CJ. In this region, curvature effects are still relatively weak such that the sonic point remains near the end of Si burning (the evolution is governed by the Si branch dynamics). However, moving further out, as the densities become lower, curvature effects rapidly become more important and are sufficient to drive the solution beyond the turning point of the Si branch, back on to the O branch. Hence, in this region the detonation speed and structure become significantly different from the planar wave. Finally, in the top-right part of the core, the curvature becomes negative due
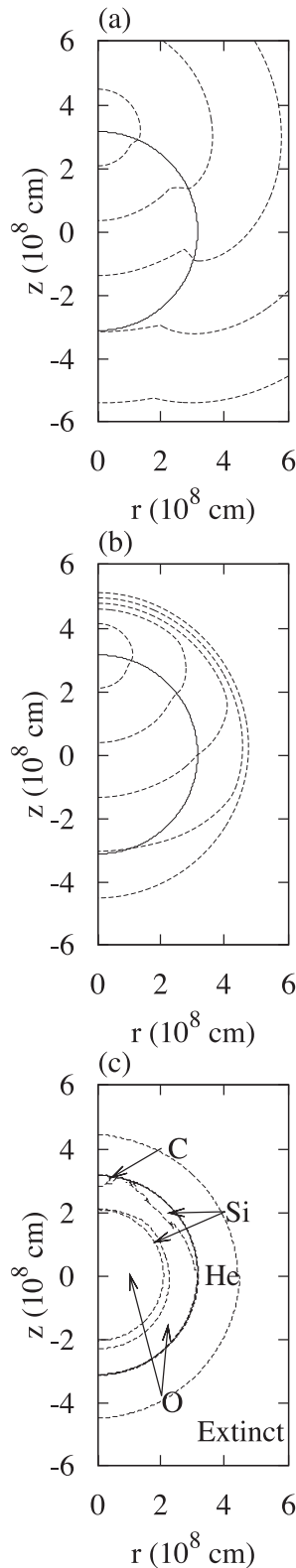
Figure 11. Case A results: (a) and (b) wave front at times 0.06, 0.21, 0.36, 0.51 and 0.66 s (dashed lines), according to PDS and DSD models, respectively; (c) DSD regimes of propagation: C, O and Si refer to the solution branch of the $D_n-\kappa$ evolution in CO, He refers to a propagating curved detonation in the shell and Extinct refers to the outer shell region where curvature has quenched the He detonation. The interface between the CO core and He shell is represented by the solid line in all plots.

to the He detonation initially driving the core detonation at the interface. In this narrow region, as the curvature decreases to zero, the solution again is driven back up to the Si branch. However, the He detonation driving effect diminishes as it travels around the core and becomes more curved and hence decelerates, such that the curvature of the CO detonation near the interface becomes positive and sufficiently high that it is driven off the Si branch in this region also. Since near the ignition 'point' the front curvature is very large and the densities are relatively low, there is a small transition region where the solution lies on the C branch. The transit time of the detonation through the core of 0.52 s is only slightly longer than that of the planar case, since the detonation speed is close to the planar values in a large part of the core.

In the core, the planar driving reaction zone lengths are less than the core radius for densities higher than $\log_{10}\rho_0 = 6.8$ g cm^{-3}, corresponding to the distance of 2.7×10^8 cm or less from the centre of the star. Further out than this, the driving zone length of the planar detonation becomes larger than the size of the core radius, and hence the assumption of complete burning breaks down. Hence in this region the PDS model is not consistent. Indeed, in the core just before the interface, these lengths are some three orders of magnitude greater than the core radius. The planar version also breaks down completely in the He. The reaction lengths are always larger than the star (for the lowest densities the He detonation length is more than 18 orders of magnitude greater than the stellar radius). However, apart from the narrow region adjacent to the interface labelled Si in Fig. 11(c) in the DSD version, the driving reaction zone lengths of the curved waves are always much less than the core radius and the density scaleheight, and hence the DSD model is self-consistent. In the narrow region mentioned above, it is likely to be unsteady, in particular where the curvature is negative at the interface, and hence a full time-dependent simulation will be required to determine the details of this part of the solution. However, since this region is small, it is not expected to have a large effect. The DSD driving reaction lengths in the He are always less than the characteristic scales of the star. The largest value is only half that of the core radius, occurring where $\log_{10}\rho_o = 5.4$ g cm^{-3} ($r = 3.8 \times 10^8$ cm).

4.2.2 Fink et al's Model 2

The next case considered is by Fink et al. (2010). They investigated whether a He detonation can later trigger a detonation in the CO core in sub-Chandrasekhar mass white dwarf explosions. They also use level set methods to pre-compute the propagation of the detonations in both He and CO, under the PDS assumption. They consider one case (Model 2) in detail. In this model, the He ignites at a point just above the base of the He envelope (at $z = 4.64 \times 10^8$ cm). Initially, only the He detonates and the wave propagates around the core and drives a shock wave into it. The shock front converges inside the core at an off-centre point. Fink et al. find that this convergence results in ignition of the CO at this point, producing a detonation which propagates outwards and consumes the CO. The density profiles of the star at the time of ignition of the He and CO detonations are shown in Fig. 12(a) and (b), respectively.

Figs 13(a) and (b) compare the wavefront arrival times for the PDS and DSD versions, respectively, for the He detonation stage of Model 2. In the evolution according to the PDS model, it takes 1.83 s for the He wave to propagate all the way around the core and converge on the axis of symmetry on the opposite side of the core to
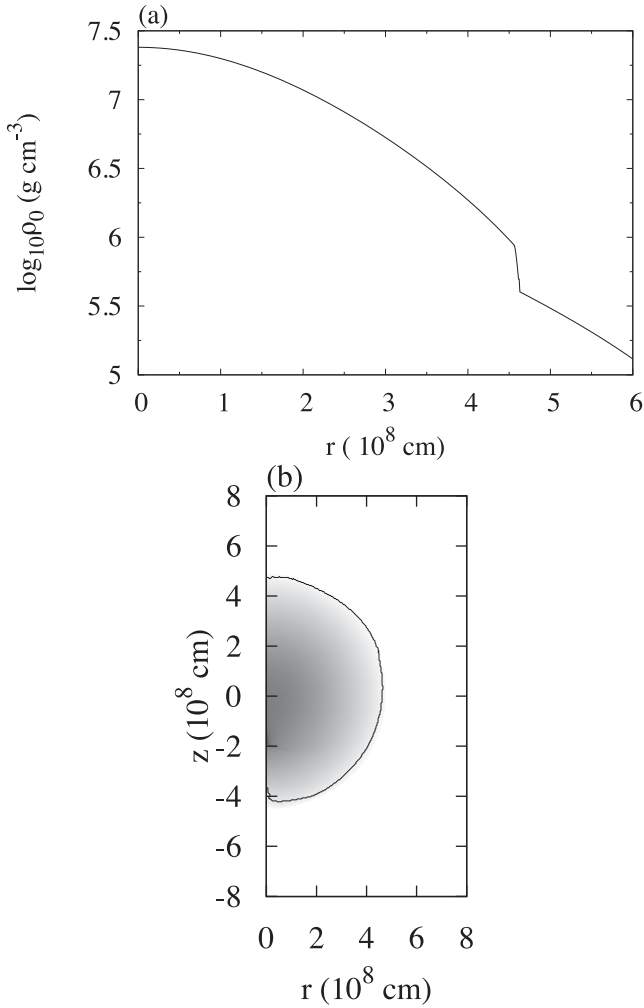
Figure 12. Density profile for model 2: (a) before first-stage He detonation and (b) before second-stage CO detonation (the scale goes from $\log_{10}\rho_o = 5.57$ g cm^{-3}, the minimum value in the core (white) to $\log_{10} = 8.13$ g cm^{-3} (black), the maximum, the solid line represents the interface).

the point of ignition ($z = -2.22 \times 10^8$ cm, Fig. 13a). In contrast, the DSD version takes 2.58 s to converge on the z-axis at $z = -4.36 \times 10^8$ cm, indicating the significant effects of curvature in this case (Fig. 13b). Indeed, the He detonation wave is sensitive to curvature in the low densities encountered in the shell and hence travels much slower than its planar version. Further out in the He envelope, due to low density it takes only a relatively small curvature to drive the detonation to extinction. In this region therefore we find that the He does not detonate. In fact, a sufficiently large 'detonation kernel' is required for detonation to be achieved. Fig. 13(c) shows that near the point of ignition, the front propagates as an inert wave and can only turn in to a detonation when the curvature becomes sufficiently small. Even then the detonation region is confined to a thin strip adjacent to the interface with the core, becoming wider as the front travels and the curvature decreases. Note that in the PDS case, there is no mechanism for extinguishing the detonation and hence the entire shell is predicted to detonate (unless an arbitrary cut-off density is employed) and hence this is qualitatively incorrect.

The planar reactions lengths in this model vary from 10^{15} to 10^{28} cm, i.e. many orders of magnitude larger than the radius of the star. The assumption of planar detonation propagation is completely
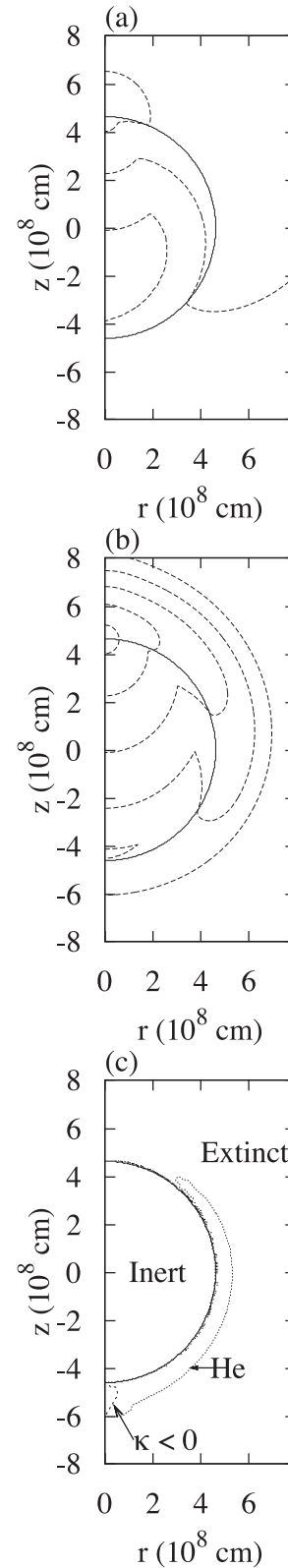

Figure 13. Model 2 He detonation stage results: (a) and (b) wave front at times 0.1,0.7, 1.3, 1.9 and 2.5 s (dashed lines), according to PDS and DSD models, respectively; (c) DSD regimes of propagation: He refers to the solution branch of the $D_n-\kappa$ evolution in He, Extinct refers to where curvature has extinguished the detonation. The negative curvature region in the He is also shown. The interface between the CO core and He shell is represented by the solid line in all plots.

invalid at any point of the evolution for this case. However, taking into account curvature, for the part of the He shell which detonates according to the DSD model, the driving zone length-scales are typically 10^5–10^7 cm. These scales are much less than the radius of the star (of the order of 10^9 cm). The DSD assumptions break down, however, near the end of the detonation of the shell due to the total curvature of the front becoming negative – note that due to axisymmetry the front is converging or imploding towards the axis and hence the cylindrical component of curvature becomes increasingly large and negative. DSD breaks down for negative curvatures (Bdzil & Stewart 2007) and hence we have reverted to PDS evolution when $\kappa < 0$. This final stage of the evolution requires a full time-dependent simulation to resolve. However, as it is only a relatively small part of the evolution near the end, it should not effect the conclusions.

We next consider the CO detonation phase of Model 2 of Fink et al. (2010). It should be noted however, as we have seen above, that taking into account curvature the He precursor detonation propagation is qualitatively different to that predicted by the PDS as employed in Fink et al. (2010). This may dramatically affect the compression and expansion waves driven into the CO core by the He detonation, and hence the core detonation ignition and evolution will take place under quite different conditions than in Fink et al's CO configuration. Indeed, while they find that the CO detonation stage is initiated due to sufficient compression in the core, the lower He DSD detonation speeds may not lead to CO ignition. However, to compute the core structure at the time of ignition (if this occurs) will require a coupled hydrodynamic evolution of the core with the curved He detonation front evolution, which is beyond the current work. Hence, here we simply consider the consequences of curvature effects on the core detonation for the original model of Fink et al. (2010) and compare with the PDS results. Figs 14(a) and (b) show the wavefront arrival times for both the PDS and DSD versions, respectively. It takes 0.54 s in the PDS version for the wave to travel through the entire CO core (Fig. 14a) but much longer, 0.98 s, in the DSD version, reflecting the significant effects of curvature. Indeed, more interestingly, due to the low densities, curvature is found to extinguish the detonation entirely in a significant band of material adjacent to the boundary with the detonated He envelope material. In fact, in the DSD version, by 0.51 s the entire detonation is extinct (Fig. 14b) and the front subsequently propagates through the remaining core as an inert wave.

Meanwhile, at the centre the wavefront is close to its planar speed due to curvature effects being least important at the relatively higher densities found there (Fig. 12b). In this region, the sonic point is located at the end of oxygen burning (Fig. 14c). As one moves out to lower densities, the underlying planar wave becomes CJ and the curvature is not sufficient to drive the solution on to the O branch. Thus, there is a narrow 'horse-shoe' shaped region of Si branch evolution. Moving out further, the densities and curvatures become such that the solution is driven back on to the O branch. Further out still, there is a significant band where the solution is driven on to the C branch, before the wave finally becomes completely extinguished in the outer regions of the core, as described above.

While the driving reaction lengths increase dramatically for the PDS version as one moves outwards to lower densities, becoming larger than the core radius at about 3×10^8 cm, the DSD theory remains self-consistent. The curvature keeps the driving zone reaction lengths much smaller than the core and density scaleheight, especially as the extinction curvatures are approached. Even when
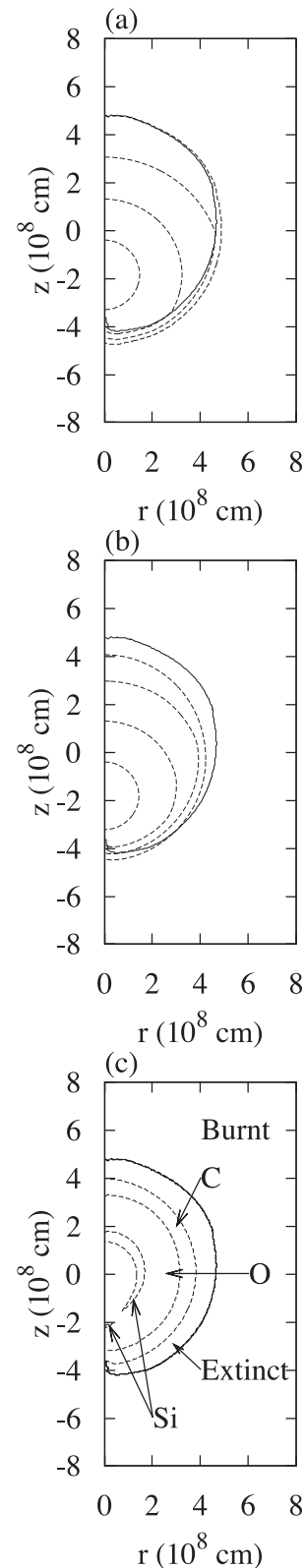

Figure 14. Model 2 CO detonation stage results: (a) and (b) wave front at times 0.09, 0.24, 0.39 and 0.54 s (dashed lines), according to the PDS and DSD models, respectively. (c) DSD regimes of propagation: C, O and Si refer to the solution branch of the $D_n - \kappa$ evolution in CO, Extinct refers to regions where the curvature has quenched the CO detonation. The interface between the CO core and products of the He detonation is represented by the solid line in all plots.

the sonic point is near the end of Si burning, the largest driving reaction length is approximately 100 times less than the core radius.

4.2.3 Y12

Model 2 investigated above demonstrates the increasing role and importance of curvature effects as the densities become lower and the reaction lengths longer. Indeed, in the lowest density regions, we have seen that front curvature effectively kills the detonation and hence in reality such regions cannot be detonated. As a final case, we hence considered a very low density delayed detonation model of Plewa (2007). Plewa (2007) investigates detonating failed deflagration models, where an explosion happens after a quenched off-centre deflagration. Only a small amount of the star is burnt in the deflagration phase and the majority of the energy expands the star. Small isolated shock-dominated regions are formed and prolonged compression leads to a detonation. One of Plewa's models in the paper, Y12, which ignites at a single point on the z-axis at $z = -2.55 \times 10^8$ cm is considered here. There is a central area of CO almost completely surrounded by the burnt material from the failed deflagration. There are pockets of CO within this burnt material. Further out there is CO material not ignited by the deflagration. Although there is a He envelope surrounding the mixture of CO and burnt material, it is far out (at a radius of the order of 10^9 cm) and the detonation front is extinct before this. Fig. 15 shows the density field of the relevant region at the time of detonation ignition (Plewa, private communication).

Figs 16(a) and (b) compare the wave front evolution according to the PDS and DSD, respectively. As before, in the PDS version (Fig. 16a), the detonation propagates through the entire computational domain since there is no extinction limit in this model. For the DSD version, initially the wave propagates as a full detonation. The downward propagating part of the detonation in Fig. 16(b) first reaches the burnt material at 0.08 s, at the point where the burnt material protrudes into the CO at $r = 4 \times 10^7$, $z = -3.64 \times 10^8$ cm. All of the wave front in the central CO region above a height of $z = -1.72 \times 10^8$ cm reaches the burnt (inert) material surrounding the central CO as a detonation. On the z-axis, the wave front reaches this burnt material at 0.34 s. As the wave front then passes through the burnt material, it emerges on the axis at 0.85 s as a C branch detonation. There are some other pockets similar to this one nearby. However, by 1.21 s the entire wave front is extinguished (including the C branch detonation pockets) and remains so. Thus in this case, when curvature effects are accounted for, only the small high-density central pocket of CO can be detonated and outside this zone, the low-density material will not be burnt. This may profoundly affect the viability of such low-density SNIa models.

Fig. 16(c) summarizes the solution branch regimes of the evolution. In terms of reaction lengths, the PDS model is only self-consistent in the central high-density regions, but becomes increasingly inconsistent as the density drops (the reaction lengths reach 16 orders of magnitude larger than the characteristic size of the CO region in the lowest densities). For the DSD case, the driving reaction lengths mostly remain below the size of the CO region and the density scaleheight. There are some regions where the reaction length exceeds the density scaleheight near the z-axis at $z = -4 \times 10^8$ cm and also in the C branch detonation pockets. However, these localized regions are very secondary in terms of mass burnt. In order to compute the details of these regions properly would require a
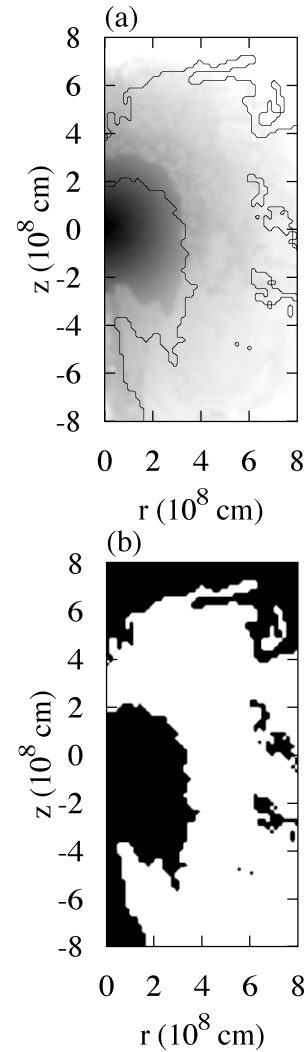

Figure 15. Density profile (a) for the model of Plewa (2007). The density is from $\log_{10}\rho_0 = 8.0$ g cm^{-3} (black) to $\log_{10}\rho_0 = 5.4$ g cm^{-3} (white). The solid line represents the interface; (b) material type for the model, where black is CO, white is burnt.

resolved time-dependent simulation. The DSD analysis shows that the scales which need resolving are very small indeed compared to the size of the star.

5 DISCUSSION

We have re-evaluated several detonation models of SNIa using DSD, which accounts for the effect of front curvature on detonation waves, including curvature-induced detonation failure. We compared the detonation wave evolution predicted by the DSD with that according to the assumption of propagation at the planar detonation speed. We have shown that, while the effects of curvature are only marginal at higher densities, these become increasingly important at lower densities. In these regions, the detonation travels slower than the planar speed, significantly affecting the wavefront arrival times, and the driving zone length (distance between the shock front and sonic point) of the detonation can be many orders of magnitude shorter than in the planar detonation wave. If the densities are low enough, the effect of curvature becomes profound in which it extinguishes
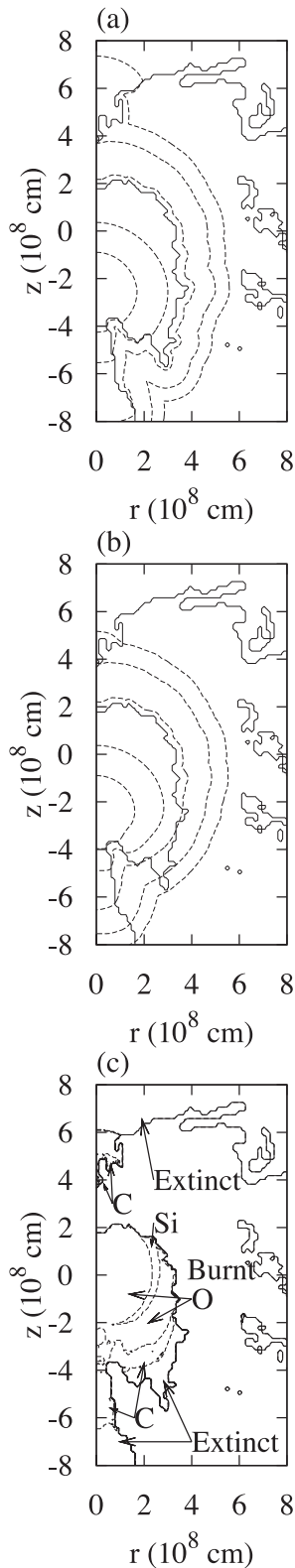
Figure 16. Y12 results: (a) and (b) wave front at times 0.11, 0.22, 0.44, 0.88 and 1.21 s (dashed lines), according to PDS and DSD models, respectively; (c) DSD regimes of propagation: C, O and Si refer to the solution branch of the $D_n - \kappa$ evolution in CO, Extinct refers to region where curvature has quenched the CO detonation. The interface between the CO core and products of the He deflagration is represented by the solid line in all plots.

the detonation altogether, whereby the shock front decays rapidly to an inert acoustic wave and the material does not subsequently burn. In the low-density regions, the planar detonation wave reaction zone lengths become orders of magnitude longer than the size of the star. While it is precisely this feature of low-density detonations which has been exploited in the various models studied here for production of intermediate-mass elements, the assumption that the wave then propagates at or closer to the planar speed is entirely inconsistent as this requires complete burning. On the other hands, the implicit DSD assumptions of quasi-one-dimensionality and quasi-steadiness are found to be self-consistent in that curvature ensures that the driving zone length typically remains smaller than the other length-scales of the problem.

In this paper, we have calculated the detonation front propagation through the star. We are currently investigating how this detonation subgrid model can be coupled to the subsequent reactive hydrodynamic evolution as has been attempted for planar speed propagation in Fink et al. (2010) and Wiggins & Falle (1997). This will allow more quantitative predictions of the effect of curvature on the composition, density, temperature and velocity fields behind the wave. These could then be used in radiation transport codes to look at the resulting light curves and spectra to re-evaluate how the various detonation models in the literature compare with observations (Höeflich & Khokhlov 1996; Nugent et al. 1997).

Nevertheless, there are a number of conclusions we can make about the consequences for nucleosynthesis and production of intermediate-mass elements in SNIa detonation models at this point. In the curved detonations, the reactions are incomplete in the driving zone length which controls the dynamics of the detonation front. While, for the lower density regions of interest, this driving zone tends to be orders of magnitude shorter than the complete planar detonation reaction length, due to the sonic point being driven to the end of O or C burning, the length- and time-scales for the completion of the reactions in the following supersonic zone will be very much longer than that of the planar wave. This is because the shock speeds and hence the temperatures are significantly lower in the curved waves than in the planar wave and the thermonuclear reactions rates are extremely temperature sensitive (Fryxell et al. 1989). This means that the reactions will be quenched due to post-detonation expansion of the star when they are much further from nuclear statistical equilibrium. In other words, taking into account the effects of curvature not only on the speed but also on the temperatures, significantly more intermediate-mass elements will be produced than predicted by arguments or models based on the planar detonations. Indeed, if the drop in detonation speed due to curvature is sufficient, the reactions could be quenched during the detonation propagation stage by α-freeze-out due to the low temperatures (Fryxell et al. 1989). Alternatively, sufficient intermediate-mass elements might be produced by sub-Chandrasekhar white dwarfs with higher densities than previously considered. Secondly, since the detonation can fail due to curvature in the outer regions of the core or the shell, this would result in a significant amount of unburnt fuel (CO or He) in the ejecta that would not be present in models where the entire core or shell is detonated and hence could qualitatively change predictions of nucleosynthesis. As mentioned in the introduction, a problem with the sub-Chandrasekhar models is the prediction of high-velocity Ni and He in the outer ejecta. Taking curvature in to account could be the solution to this problem as the production of iron group elements decreases due to much lower detonation speeds and temperatures (Fink, private communication). Conversely

however, if little of the He detonates in the envelope, this could lead to a large increase of He in the outer ejecta.

The $D_n-\kappa$ curves used in this paper were generated by Sharpe using an α-network of 13 species with 27 reactions. Messoudi et al. (2009) used a full reaction network of 331 species and 3262 reactions and compared the curve they obtain for $\rho_0 = 5 \times 10^6$ g cm^{-3} with that of a 13 species and 18 reactions α-network. They find that the full reaction network gives faster speeds and greater residue of Si and production of Ni. Messoudi et al. (2009) find the extinction curvature of the C branch an order of magnitude higher. Assuming this is true for all $D_n-\kappa$ curves and to the same degree, the regions where the sonic point is in Si or C could possibly be shifted further out from the core centre. The detonation would also travel slightly further before becoming extinguished. However, even if the extinction curvatures are an order of magnitude higher, this would still be sufficient to ensure detonation failure for low densities. Hence, while the choice of reaction network may quantitatively affect the predictions, it will be a minor effect compared to the very large qualitative difference between taking into account curvature and not doing so. We will investigate this in the future.

The local curved detonation wave properties and the pre-computed front propagation for the several examples considered are intended to provide not only a priori bounds on the length- and time-scales which need to be resolved in any SNIa simulation, but also benchmarks against which other simulation methods may be compared. It is to be emphasized that, since it is the detonation structure itself which determines the dynamics and evolution, to obtain even qualitatively good results of detonation propagation, one must resolve the driving part of the structure, whether by sufficiently fine gridding or by subgrid resolution DSD methods. A resolution too low results in unacceptable errors; even a grid spacing which is one order of magnitude less than the driving zone length is often usually not enough to even approach well-converged solutions (Aslam et al. 1998; Sharpe & Braithwaite 2005). It is precisely this reason why the development of rigorous DSD-type methods was essential, and why these are now the mainstay of engineering explosives codes (Bdzil & Stewart 2007). The situation is in fact much worse for SNIa simulation as the disparity in length-scales is much larger than in typical engineering applications. This means that in practice detonations in full star direct simulations are necessarily not only underresolved, but often *unresolved*, i.e. the grid sizes, numerical shock structures and numerical burning zones can be order of magnitudes larger than the actual scales. These numerical solution structures may have completely different dynamics to the solutions of the governing equations (Menikoff, Lackner & Bukiet 1996).

Furthermore, even if the 'consistency' check on the leading-order DSD solutions demonstrate that the quasi-steady approximation is in fact violated in large parts of the star for a given scenario, this in itself is an important finding, as then scales smaller than those of the DSD driving zones need to be resolved. It should be noted that the requirements for capturing such highly dynamic or truly transient regions are very much more stringent than for correctly computing quasi-steady detonation solution discussed above. Indeed, extremely fine resolution is then required to obtain even the qualitatively correct solutions numerically (Kapila et al. 2007). Computing correctly detonation ignition and failure in a full star simulation thus represents a very considerable challenge.

REFERENCES

Arnett W. D., 1969, Astrophys. Space Sci., 5, 180
Aslam T. D., Bdzil B. B., Stewart D. S., 1996, J. Comp. Phys., 126, 390
Aslam T. D., Bdzil J. B., Hill L. G., 1998, In Proc. Of 11th International Detonation Symposium. Extension to DSD Theory: Analysis of PBX 9502 Rate Stick Data. Detonation, Snowmass, CO, Office of Naval Research, Arlington, VA, p. 21
Bdzil J. B., Aslam T. D., 2000, Los Alamos National Laboratory Report, LA-UR-00-942
Bdzil J. B., Stewart D. S., 2007, Annu. Rev. Fluid Mech., 39, 263
Branch D., Lacy C. H., McCall M. L., Sutherland P. G., Uomoto A., Wheeler J. C., Wills B. J., 1983, ApJ, 270, 123
Colgate S. A., McKee C., 1969, ApJ, 157, 623
Fickett W. D., Davis W. C., 1979, Detonation. University of California Press, Berkeley
Fink M., Röpke F. K., Hillebrandt W., Seitenzahl I. R., Sim S. A., Kromer M., 2010, A&A, 514, A53
Fryxell B. A., Müller E., Arnett D. A., 1989, Technical Report, Hydrodynamics and Nuclear Burning. Max-Plank Institut für Physik und Astrophysik, Garching
Gamezo V. N., Wheeler J. C., Khokhlov A. M., Oran E. S., 1999, ApJ, 512, 827
Hillebrandt W., Niemeyer C. J., 2000, Annu. Rev. Astron. Astrophys., 38, 191
Höeflich P., Khokhlov A., 1996, ApJ, 457, 500
Kapila A. K., Schwendeman D. W., Bdzil J. B., Henshaw W. D., 2007, Combust. Theor. Model., 11, 781
Khokhlov A. M., 1989, MNRAS, 239, 785
Khokhlov A. M., 1991, A&A, 245, 114
Menikoff R., Lackner K. S., Bukiet B. G., 1996, Combust. Flame, 104, 219
Messoudi A. E., Vidal P., Busegnies Y., 2009, C. R. Mec., 335, 768
Nomoto K., 1982, ApJ, 257, 780
Nugent P., Baron E., Branch D., Fisher A., Hauschildt P. H., 1997, ApJ, 485, 812
Plewa T., 2007, ApJ, 657, 942
Sethian J. A., 1999, Level Set Methods and Fast Marching Methods, Cambridge Univ. Press, Cambridge
Sharpe G. J., 1999, MNRAS, 310, 1039
Sharpe G. J., 2000a, Combust. Flame, 123, 68
Sharpe G. J., 2000b, Phys. Fluids, 12, 3007
Sharpe G. J., 2001, MNRAS, 322, 614
Sharpe G. J., Braithwaite M., 2005, J. Eng. Math., 53, 39
Stewart D. S., 1998, in Burgess A. R., Dryer F. L., eds, Twenty-Seventh Symposium (International) Combustion. Combustion Institute, Pittsburgh, PA, p. 2189
Stewart D. S., Yao J., 1998, Combust. Flame, 113, 224
Townsley D. M., Jackson A. P., Calder A. C., Chamulak D. A., Brown E. F., Timmes F. X., 2009, ApJ, 701, 1582
Wheeler J. C., Harkness R. P., 1990, Rep. Prog. Phys., 53, 1467
Wiggins D. J. R., Falle S. A. E. G., 1997, MNRAS, 287, 575
Woosley S. E., Weaver T. A., 1994, ApJ, 423, 371

This paper has been typeset from a TeX/LaTeX file prepared by the author.